



Supplementary Material for:
Temporal variations in storage conditions of the post-collapse rhyolites,
Valles Caldera, New Mexico (USA)

 Magdalen A. Grismer*^α and  Laura E. Waters^α

^α Department of Earth and Environmental Science, New Mexico Institute of Mining and Technology, Socorro, NM 87801, USA.

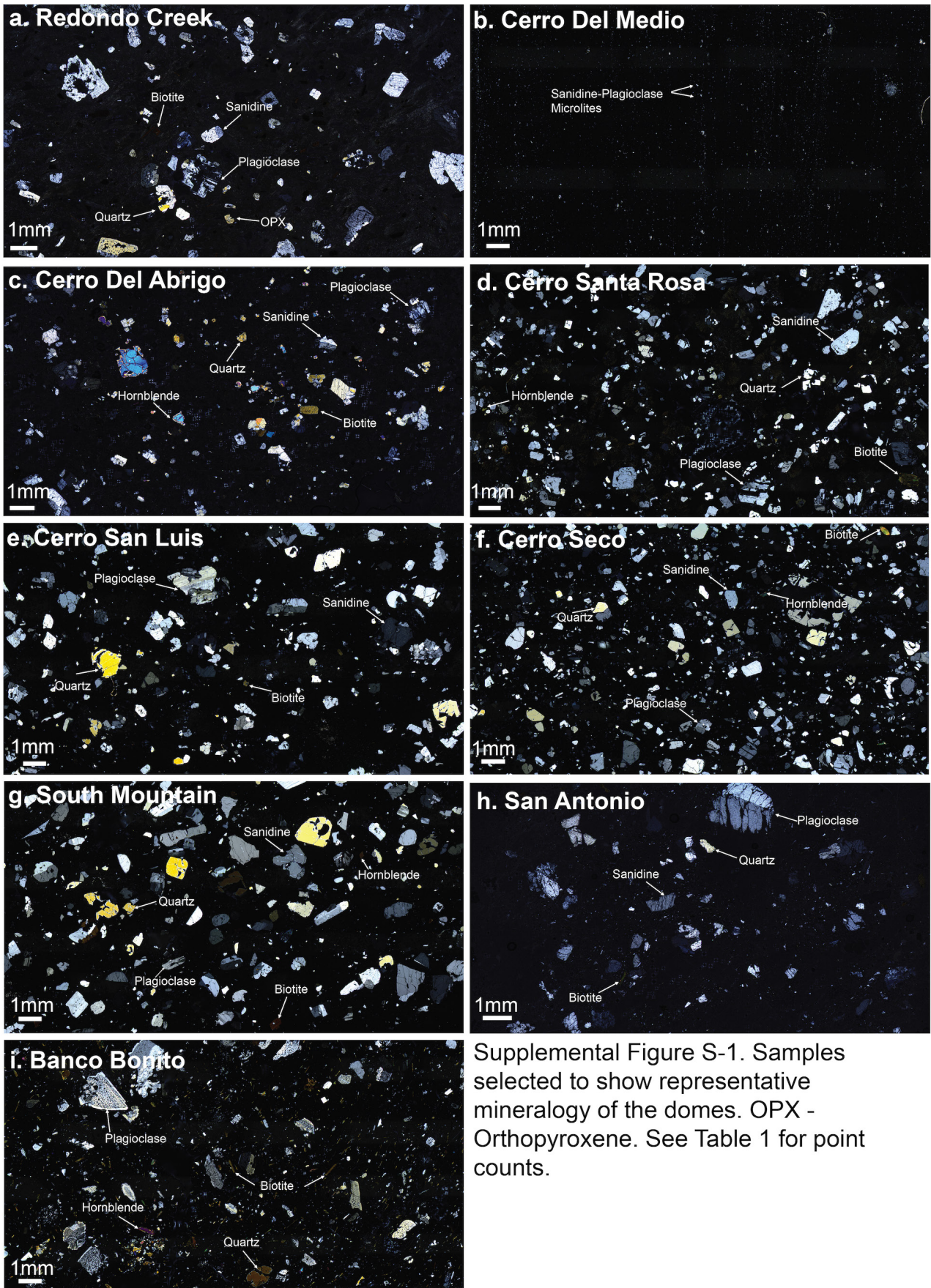
This supplementary material accompanies the article:

Grismer, M. A. and Waters, L. E. (2024) “Temporal variations in storage conditions of the post-collapse rhyolites, Valles Caldera, New Mexico (USA)”, *Volcanica*, 7(1), pp. 303–333. DOI: <https://doi.org/10.30909/vol.07.01.303333>.

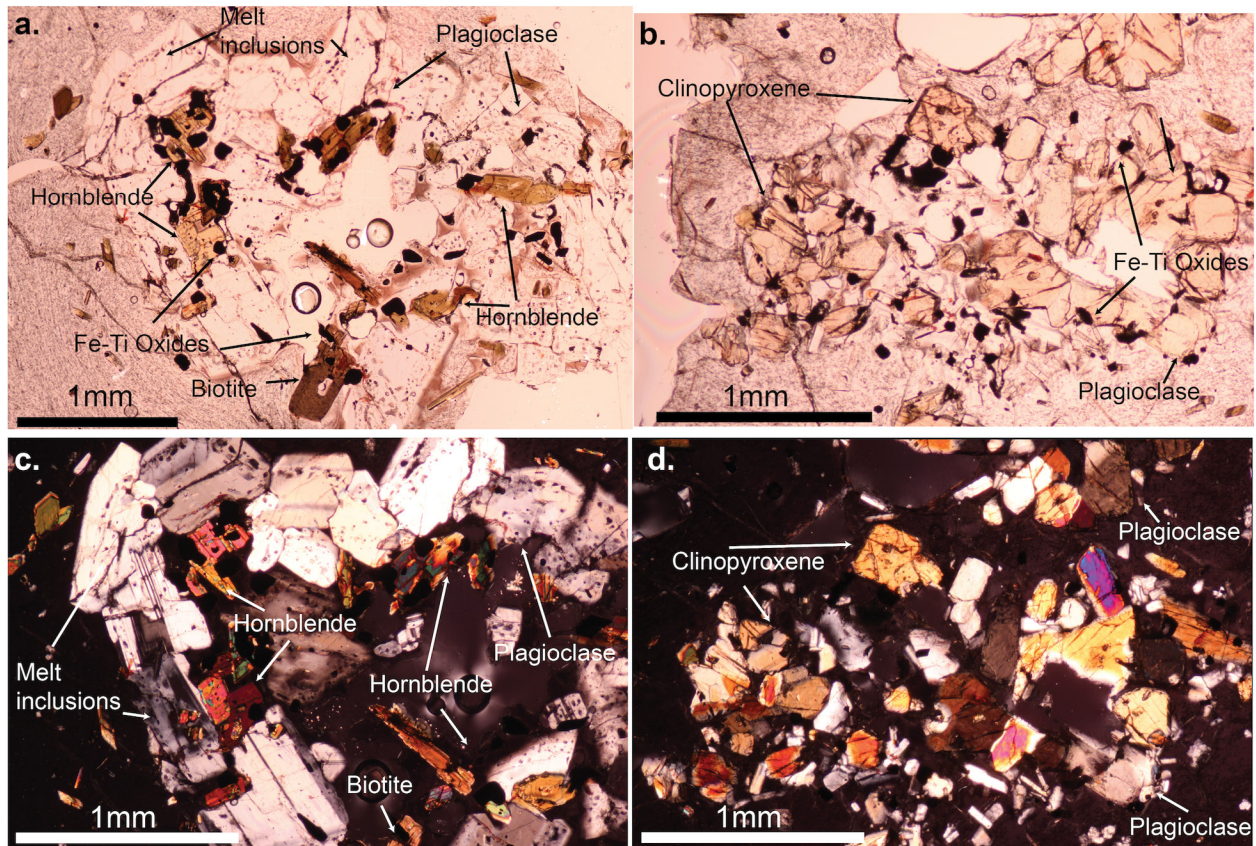
Grismer & Waters (2024) should be cited if this material is used independently of the article.

COPYRIGHT

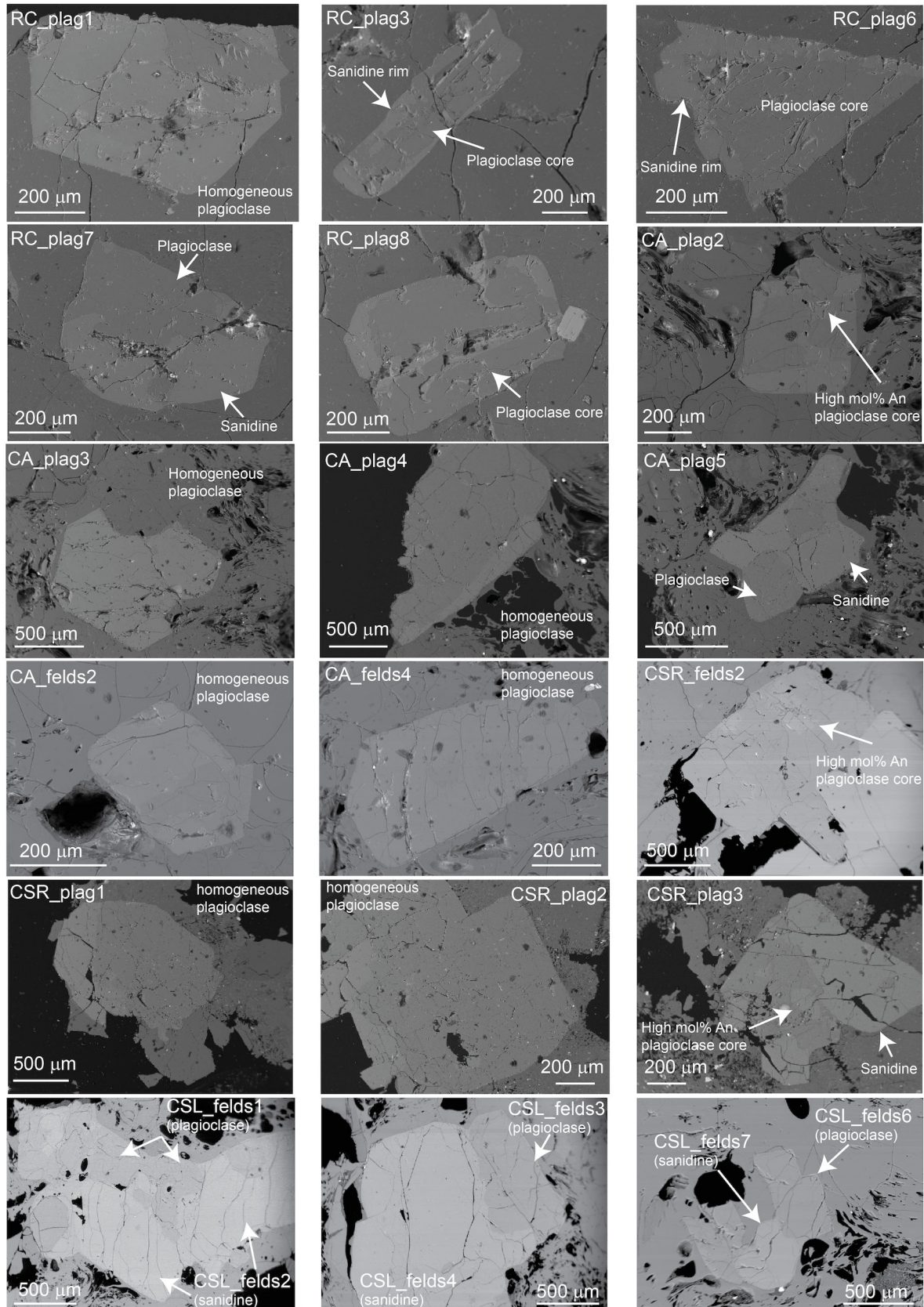
© The Author(s) 2024. This article is distributed under the terms of the [Creative Commons Attribution 4.0 International License](#), which permits unrestricted use, distribution, and reproduction in any medium, provided you give appropriate credit to the original author(s) and the source, provide a link to the Creative Commons license, and indicate if changes were made.



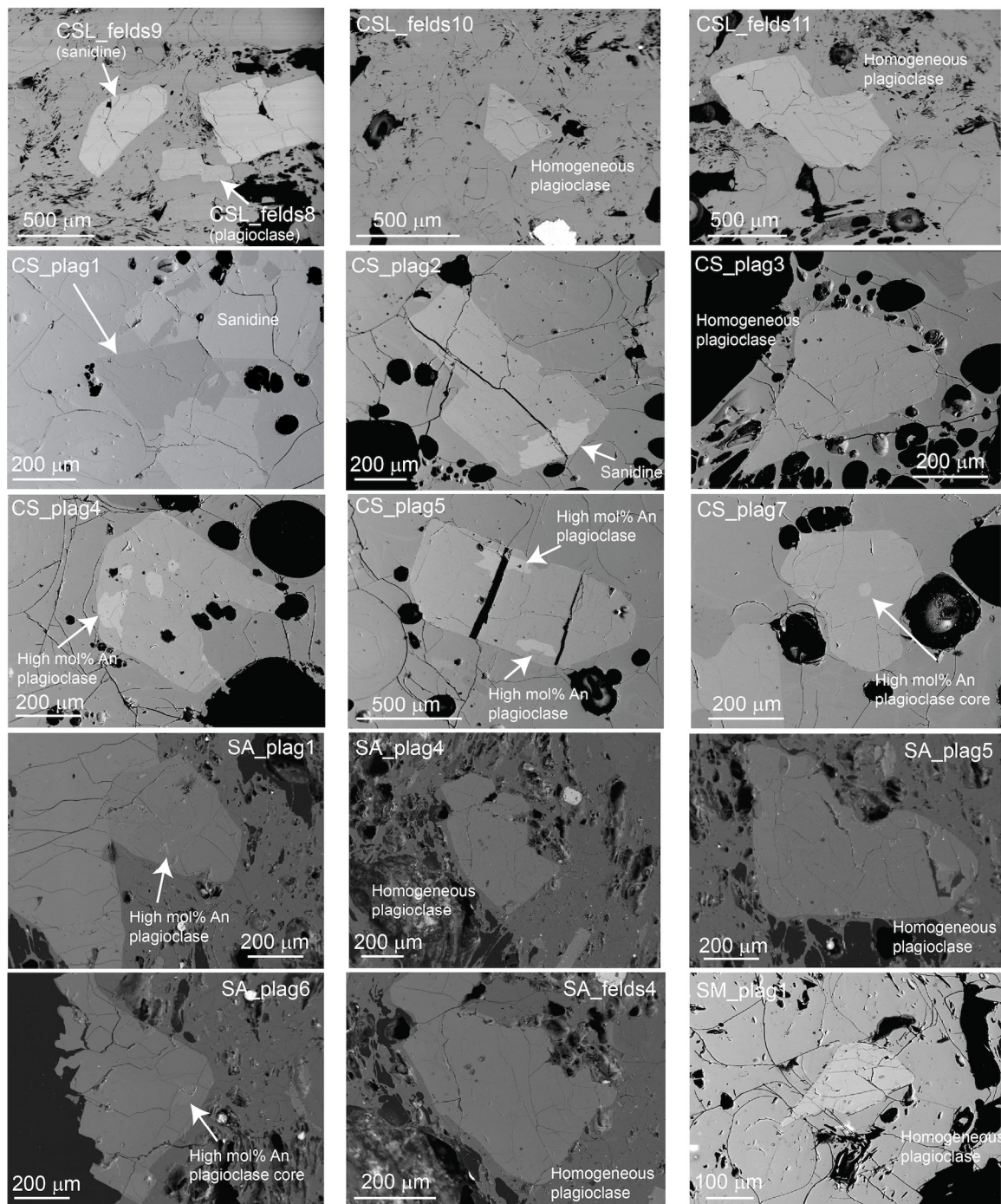
Supplemental Figure S-1. Samples selected to show representative mineralogy of the domes. OPX - Orthopyroxene. See Table 1 for point counts.



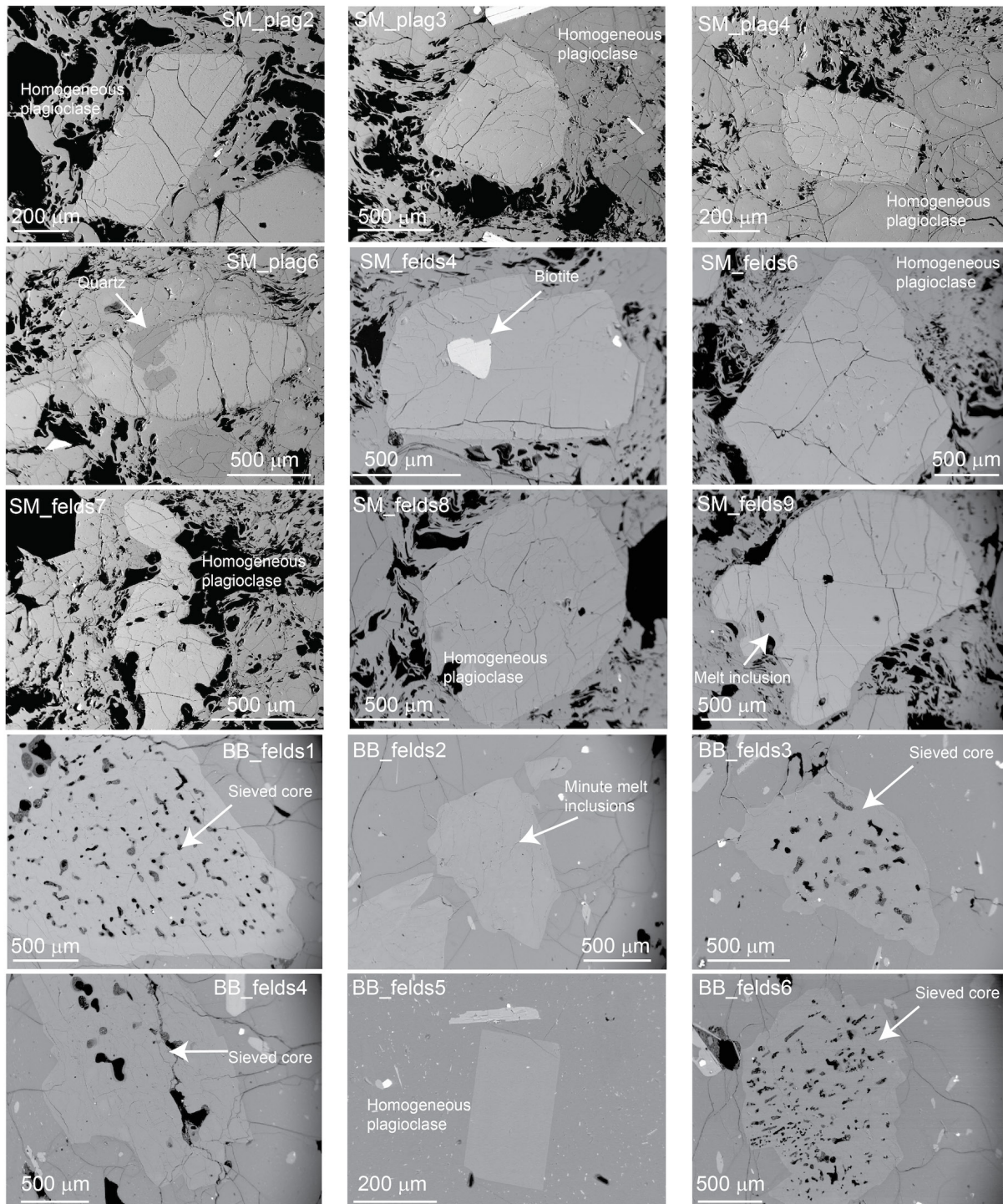
Supplemental Figure S-2. Photomicrographs of the two varieties of crystalline inclusions in Banco Bonito. (a, c) Granitoid crystalline inclusion in PPL and XPL respectively, comprised of abundant plagioclase, hornblende and biotite, with trace Fe-Ti oxides. Melt inclusions are visible in the plagioclase crystals surrounding the clot, forming a melt rim around the inclusion. (b, d) Spinel-gabbro crystalline inclusion in PPL and XPL respectively, comprised of abundant clinopyroxene and plagioclase, with trace Fe-Ti oxides.



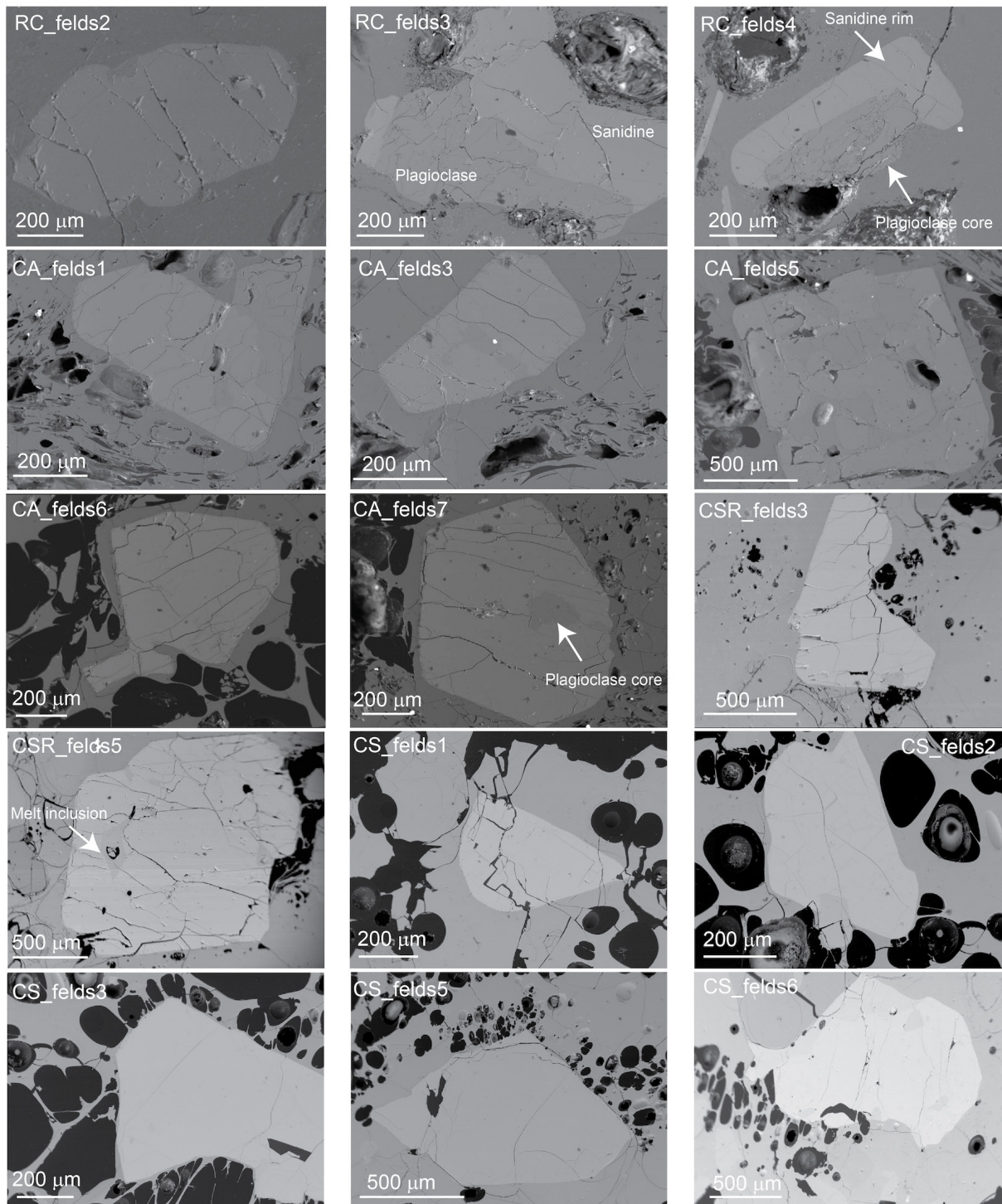
Supplemental Figure S-3. Plagioclase BSE images to showcase textures and habits, gray scale has been modified to better differentiate crystals from the groundmass, the majority of plagioclase crystals are homogeneous, though some contain calcic cores, sanidine is often found on the margins.



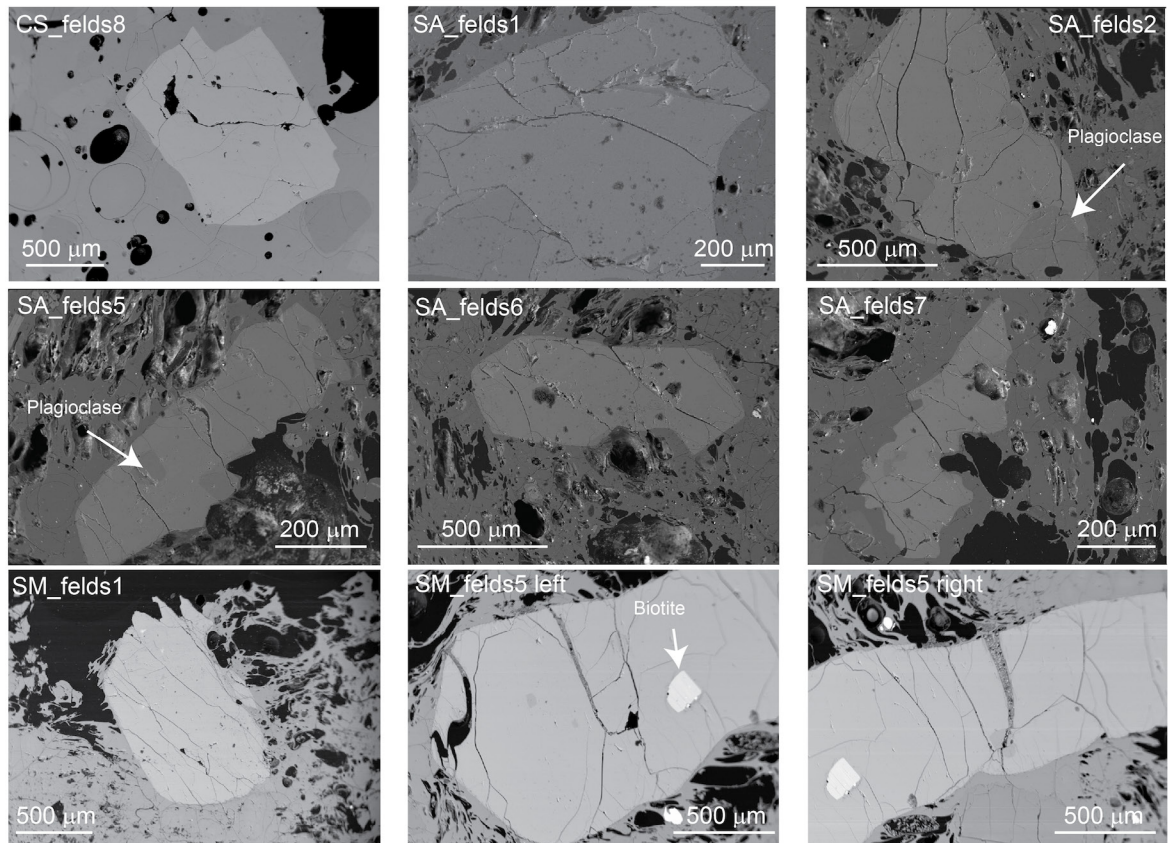
Supplemental Figure S-4. Additional plagioclase BSE images, plagioclase in San Luis is homogeneous, and almost exclusively found with sanidine on the margins. Seco and San Antonio both contain calcic cores plagioclase samples.



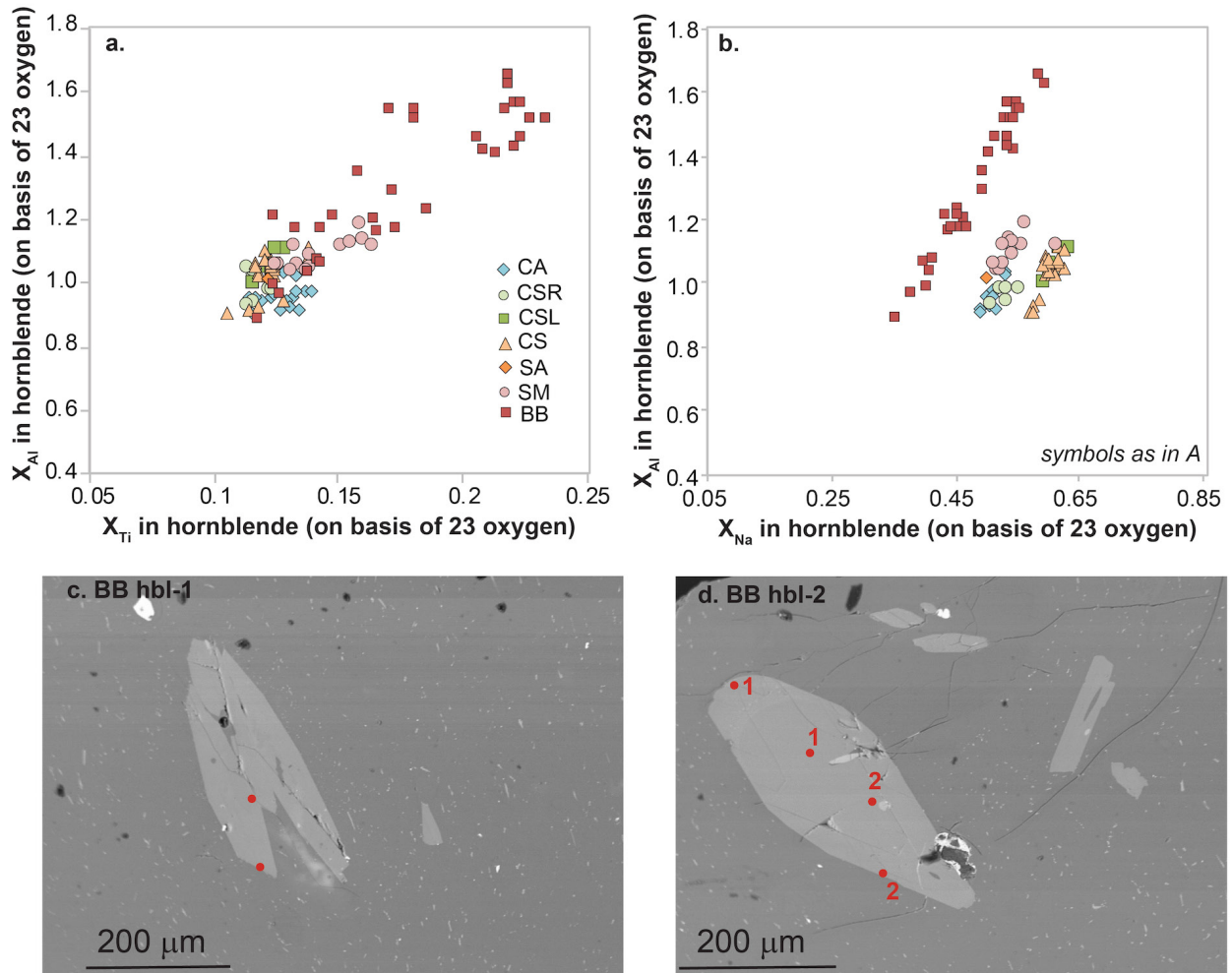
Supplemental Figure S-5. Additional plagioclase BSE images. South Mountain contains predominantly homogeneous plagioclase, but has trace melt inclusions, as well as quartz, and in one instance biotite cores. Plagioclase in Banco Bonito is typically heavily sieved, though there are instances of homogeneous crystals, and cores with trace melt inclusions.



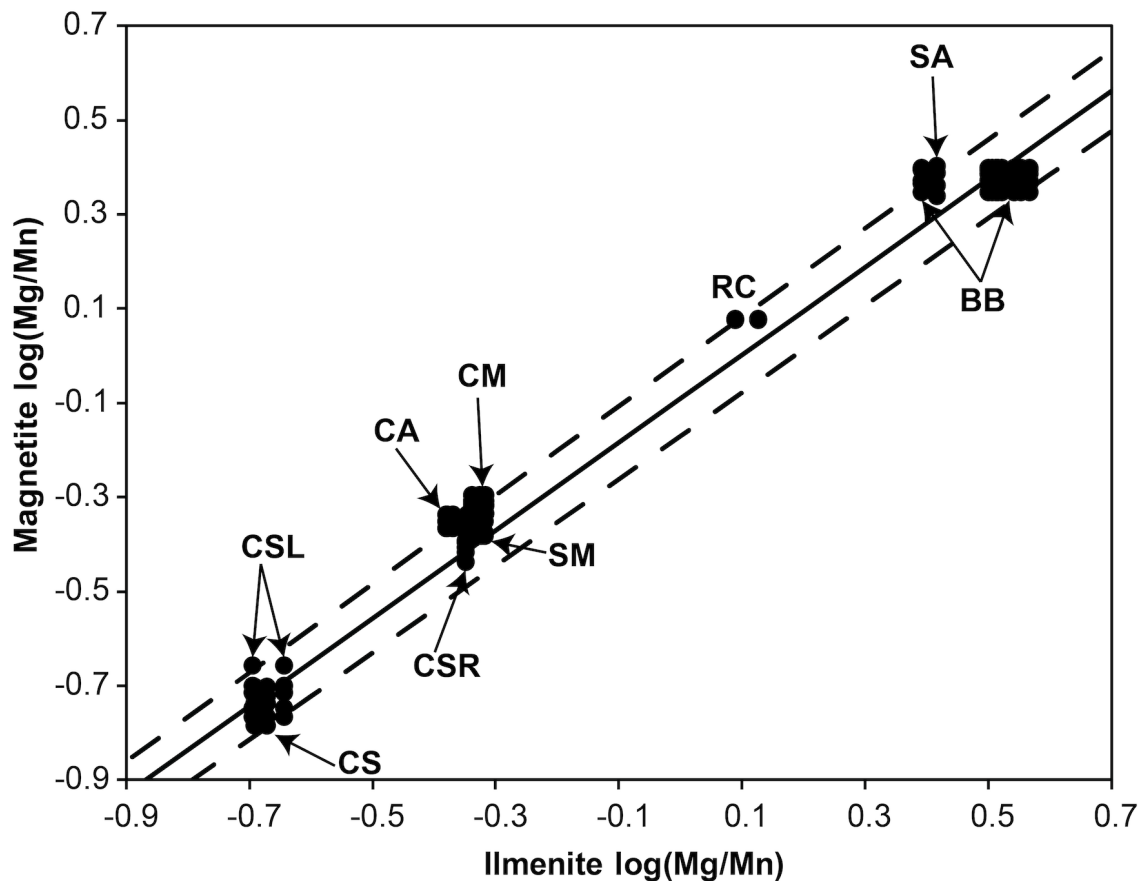
Supplemental Figure S-6. Sanidine BSE images, grayscale in the images adjusted to differentiate crystals from groundmass more easily, all crystals without notation are compositionally homogenous. Sanidine in all the post-collapse domes is primarily homogeneous and in many cases found next to, or growing on the margins of plagioclase. Redondo Creek contains trace sanidine with plagioclase cores. In Abrigo we see one instance of a small, relict plagioclase core, and a melt inclusion in Santa Rosa.



Supplemental Figure S-7. Additional sanidine BSE images. Plagioclase is present in the margins and intergrown with several sanidine crystals in San Antonio, and in one instance a biotite crystal is seen in a sanidine phenocryst in South Mountain. Again, within each dome sanidine is compositionally homogeneous.

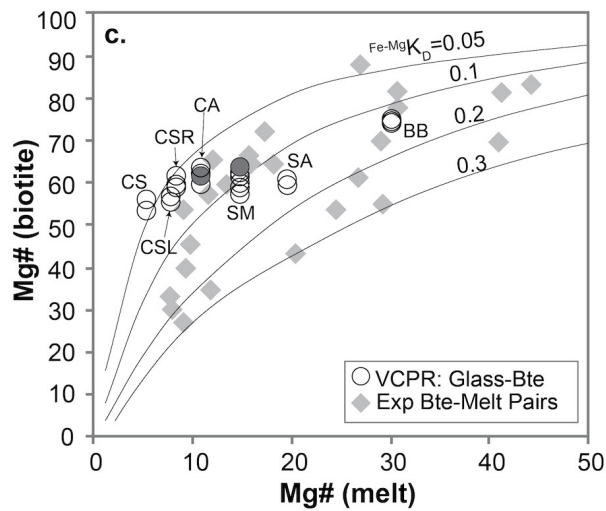


Supplemental Fig S-8: a) X_{Al} v. X_{Ti} in hornblende in the post-collapse rhyolites, note the comparatively consistent values in all the domes, except for Banco Bonito (red squares). b) X_{Al} v. X_{Na} in the post-collapse rhyolites, again note the comparatively consistent values in all the domes, except for Banco Bonito (red squares). c) Hornblende crystal in Banco Bonito that appears homogeneous under BSE imaging, where the core records a pressure of 157 MPa, and the rim records a pressure of 308 MPa, analyses indicated by red points. d) A second, similarly sized, hornblende from Banco Bonito where two pairs of core-rim analyses were taken, with the first core-rim pair (labeled 1) recording pressures of 199 MPa, and 224 MPa respectively; and the second core-rim pair (labeled 2) recording 189 MPa and 223 MPa respectively.



Supplemental Figure S-9.

Shown above is a plot of $\text{Mg}/\text{Mn}_{\text{Ilmenite}}$ v. $\text{Mg}/\text{Mn}_{\text{Magnetite}}$ for all possible pairs of ilmenite and magnetite and the test of equilibrium (solid line) proposed by Bacon & Hirschmann (1988). 2σ lines are dashed, any pairing that lies between the 2σ variation is considered in equilibrium. Only pairs that passed this test were used to calculate pre-eruptive temperatures. There is considerable overlap in composition between the HSRs (Cerro San Luis (CSL) and Cerro Seco (CS); and Cerro Del Medio (CM), Cerro Del Abrigo (CA), Cerro Santa Rosa (CSR), and South Mountain (SM)) and the LSRs (San Antonio (SA) and Banco Bonito (BB)).



Supplemental Figure S-10.

Biotite equilibrium test, Mg# in the melt shown relative to Mg# in biotite, with $Fe-MgK_D$ values shown as black lines, and the post-collapse domes shown in grey. Experimental values (gray diamonds) (Carmichael & Nicholls, 1967; Holtz, 2004; Lukkari & Holtz, 2007; Mutch et al., 2016; Righter & Carmichael, 1996; Sato, 2004; Tomiya et al., 2010). All biotite in the post-collapse domes overlaps with experimental data.